Optoelectronic Modelling, Circuit Design and Modulation for Polymer-Light Emitting Diodes for Visible Light Communication Systems

Andrew Burton[4], Alessandro Minotto[3], Paul Anthony Haigh[1,2],
Zabih Ghassemlooy[4], Hoa Le Minh[4], Franco Cacialli[3] and Izzat Darwazeh[1]
[1]Communications and Information Systems, University College London, Gower Street, London, WC1E 6BT, UK
[2]Photonics Innovations Laboratory, University College London, Gower Street, London, WC1E 6BT, UK
[3]Department of Physics and Astronomy, University College London, Gower Street, London, WC1E 6BT, UK
[4]Optical Communications Research Group, Northumbria University, Newcastle-upon-Tyne, NE1 8ST, UK
{andrew2.burton; z.ghassemlooy; hoa.le-minh}@northumbria.ac.uk; {p.haigh; a.minotto; i.papakonstantinou; f.cacialli; i.darwazeh}@ucl.ac.uk

***Abstract*—This paper investigates the use of organic polymer light emitting diodes (PLEDs) for the use in visible light communications (VLC). We prepared blue and green emitting PLEDs using commercial light-emitting polymers, and then characterised the device emission (spectrum and power), and extracted their circuit parameters for their electrical equivalent model for driving with small signals. In addition, we characterised the bandwidth (B_{mod}) of the devices over a period of continuous driving (~ 4 h) and found that for the blue PLEDs the B_{mod} decreased from an initial 750 kHz to a steady state of ~250 kHz. The green-emitting devices were found to benefit from an extended B_{mod} of ~1.5 MHz at the beginning of the test, which then stabilised to ~850 kHz. Furthermore, with the addition of a first order RC filter we show that, the steady state B_{mod} of the blue PLED cane be increased by a factor of ~3, thus allowing > 1 Mbps non-return to zero on-off keying (NRZ OOK) data transmission in a complete VLC system.**

Keywords—circuit design, modelling, modulation, organic light-emitting didoes, visible light communications

I. Introduction

Organic polymer-based light-emitting diodes (PLEDs) are an attractive proposition for visible light communication (VLC) systems. They are produced at very low costs via wet processing methods into arbitrarily large photoactive areas on flexible substrates [1]. These advantages enable new applications, where PLEDs are ideally suited to, such as large area ceiling and display panel lights, or displays in smart devices.

However, PLED devices face several challenges in comparison to the inorganic LEDs, including lower optical power and significantly lower charge mobility [2]. Low mobility's directly lead to lower modulation bandwidths (B_{mod}), for similar device geometry, similarly to inorganic LEDs. Although high B_{mod} has been demonstrated (26 MHz) [3], in most reported VLC links in the literature B_{mod} is in the range of hundreds of kHz [4] in order to ensure sufficient optical power level. In order to address bandwidth limitation, a number of schemes have been reported in the literature including (*i*) pre- and post-equalization; (*ii*) parallel transmission (i.e., multiple inputs multi outputs); multi-level and multi-carrier modulation formats such as orthogonal frequency division multiplexing (OFDM) with a transmission data rate R_b of 51.6 Mb/s [5]; and wavelength division multiplexing (WDM). In [4], on-off keying (OOK) WDM VLC with PLEDs and artificial neural network (ANN)-based equalizer was used to demonstrated R_b of 55 Mb/s [4].

While relatively high R_b have been achieved, there have been few reports in the literature on full communications system-based optoelectronic characterisation of PLED devices. In this work, we fully characterise PLED devices developed at University College London (UCL) for use VLC in terms of light-current and current-voltage relationships, bandwidth/rise-time measurements and electrical signal model. We have developed a simple equaliser, which extends the B_{mod} to >750 kHz, an improvement of ~3 over the raw B_{mod} (~250 kHz). Furthermore, we analyse the device stability over time, alongside complete VLC system measurements of data throughput and the bit error rate (BER) performance for a non-return-to-zero OOK (NRZ-OOK) VLC link.

The rest of this paper is organised as follows: the design of the PLEDs and their DC performance is given in Section II. Section III covers the device model, rise time and bandwidth measurements. Section IV investigates the device stability over time and Section V looks at data transmission. Conclusions are drawn in Section VI.

II. Polymer Light-Emitting Diode Fabrication

The PLEDs reported here were fabricated on commercial glass substrates patterned with indium tin oxide (ITO) as transparent anodes (OSSILA Ltd), which were treated in an oxygen-plasma chamber for 10 minutes [6, 7]. To facilitate the injection of holes, a 40 nm layer of poly (3,4-ethylenedioxythiophene) - poly (styrenesulfonate) (PEDOT:PSS) was spin-casted onto the ITO substrates from a water dispersion (Heraeus Clevios™ AI 4083) in air and

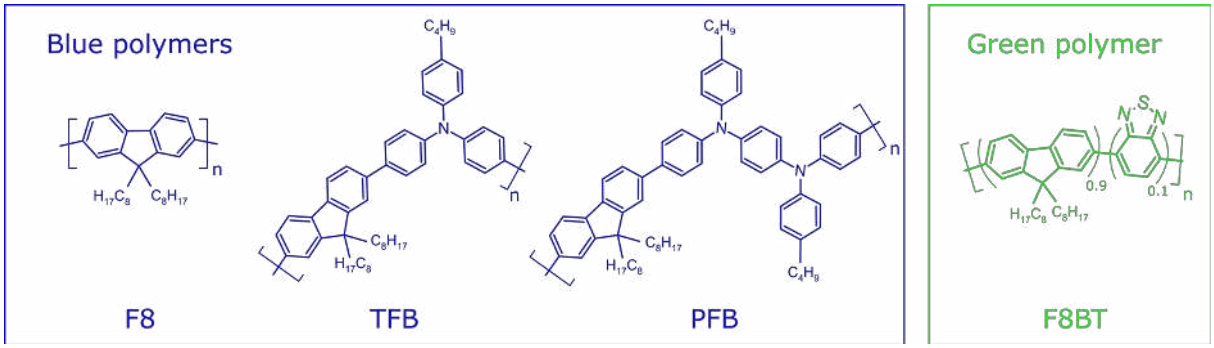

Fig. 1 Molecular structures of the light-emitting polymers. All polymers were purchased from American Dye Source

thermally annealed in a nitrogen-filled glove-box at 150 °C for 10 minutes.

On top of the annealed PEDOT:PSS, a ~100 nm thick emissive layer was spin-casted in the glove-box from 10 mg/mL toluene solutions of either the green-emitting poly(9,9-dioctylfluorene-co-benzothiadiazole) (F8BT, with 10 % of benzothiadiazole loading) copolymer or a blend of three blue-emitting polymers: poly(9,9-dioctyluorene) (F8), (poly(9,9-dioctyluorene-alt-N-(4-butylphenyl)diphenylamine) (TFB) and poly(9,9-dioctyluorene-alt-bis-N,N'-(4-butylphenyl)-bis-N,N'-phenyl-1,4-phenylenediamine) (PFB), in a 1:2:2 ratio. The molecular structures of the light-emitting polymers are illustrated in Fig. 1.

Following this, cathodes consisting of calcium (30 nm) with an aluminium layer (200 nm thickness) were thermally evaporated on top of the emitting polymer layer in a high-vacuum chamber. Finally, the PLEDs were encapsulated in the glove-box by depositing a UV-curable epoxy glue (OSSILA Ltd) layer covered with a protective glass slide. Each device consists of six independent pixels with an active area of 4.5 mm^2 per device as defined by the overlap between the patterns of the bottom (ITO) and the top (Ca/Al) electrode.

Typical electroluminescence (EL) spectra of both blue and green PLEDs, and the corresponding current density/radiance versus bias voltage (JVR) plots are depicted in Fig. 2. As illustrated in Fig. 2(a), the EL of the blue PLEDs is characterised by two vibronic components, peaking at 455 and 482 nm, and a weaker and broader shoulder at about 600 nm, which could be ascribed to the formation of charge and exciton trapping "keto-defect" sites, as described in previous works [8, 9]. Looking at the blue device characteristics (Fig. 2(b)), a turn-on voltage (V_{ON}, defined as the voltage at which the light output exceeds the noise level) as low as 2.8 V could be measured, with a maximum radiance reaching up to 2.7 mW/cm^2, corresponding to 1,875 Cd/m^2 luminance (measured at 11 V) and a maximum external quantum efficiency (EQE) of 0.25 %.

In Fig. 2(c), the emission spectrum from a green PLED is illustrated. The EL peaks at 540 nm, with no evidence of emission from a low-energy oxidised species. Indeed, the green-emitting polyfluorene employed here (F8BT) [10] is less affected by oxidative processes due to its higher ionisation potential (IP ~ 5.9 eV) compared to the blue-emitting TFB and PFB (IP ~ 5.3 and 5.1, respectively) [11]. Thanks to this, and to the higher photoluminescence quantum yield (PLQY = 66 %) of F8BT (measured in air using an integrating sphere setup and following a protocol reported in the literature [12]) compared to the blue-emitting blend (PLQY = 10 %), green PLEDs exhibited about three times higher radiance (up to 8.6 mW/cm^2, measured at 9.6 V and corresponding to a 13,453 Cd/m^2 luminance) and five times higher maximum EQE of 1.27%. As for the blue PLEDs, the measured V_{ON} is also ~2.8 V.

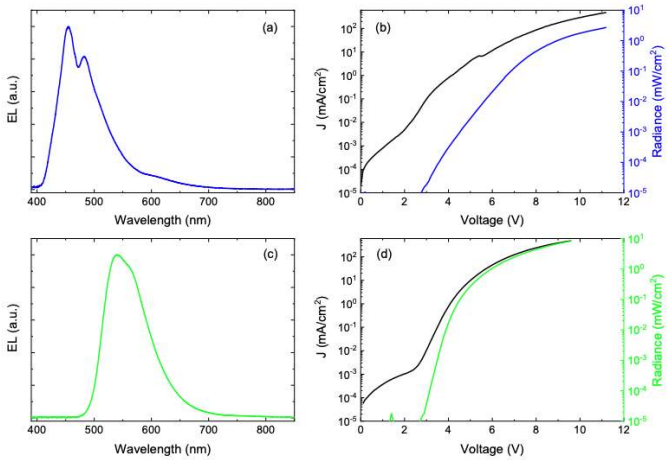

Fig. 2 EL spectra and semilog JVR plots of blue (a,b) and green (c,d) PLEDs. The EL spectra were collected at 2 mA of current bias (J ~ 44 mA/cm^2). The turn-on voltage for both the blue and the green PLEDs is 2.8 V, obtained by intersecting the radiance data (b,d) with the noise level of our photodetector (10^{-5} mW/cm^2) The samples were characterised using a Keithley 2400 source meter for both the current measurement and the voltage/current supply. The optical output of the PLEDs was measured with a calibrated silicon photodiode and the EL spectra were collected using an Andor Shamrock 163 spectrograph coupled with an Andor Newton electron-multiplying charge-coupled device

III. Characterisation for Communications

Understanding the AC performance of the PLED devices under test (DUT) is necessary in order to optimise their utilisation in a communications system. The equivalent small signal circuit of the fabricated PLED shown in Fig. 3(b) is depicted in Fig. 3(a). The circuit is composed of a device contact resistance R_s in series with the diode, and an RC low-pass filter (LPF) consisting of the bulk resistance R_p in parallel with the equivalent bulk capacitance C_p.

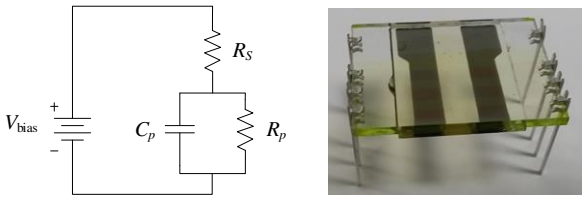

(a) (b)

Fig. 3 (a) PLED equivalent circuit and (b) photograph of the PLED with six pixels, each pixel measuring 4.5 mm^2

Analysis of the equivalent circuit reveals that the voltage across C_p is defined by [13]:

$$V_{C_p}(t) = V_b\left(1 - e^{\frac{-t}{C_p R_p}}\right) \quad (1)$$

where V_b is the dc bias voltage, C_pR_p is the device time constant, t is the instantaneous time and C_p is defined by [13]:

$$C_p = \varepsilon_0 \varepsilon_r \frac{A}{d} \quad (2)$$

where ε_0 and ε_r are the permittivity of free space and the dielectric constant of the emissive material, respectively, A and d represent the photoactive cross-sectional surface area and device thickness, respectively.

The PLED electrical cut-off frequency f_c can be expressed as:

$$f_c = \frac{1}{2\pi R_p C_p} \quad (3)$$

Clearly, devices with increasing photoactive area (or decreasing thickness) are inherently associated with a higher equivalent capacitance C_p. By substitution of (2) into (3), the available modulation bandwidth is dependent on the device geometry. As mentioned, the devices used in this work have a photoactive area of 4.5 mm^2. We estimate the equivalent circuit component values by using a Keysight vector network analyser (VNA-E5061B) to measure the blue PLED impedance between 50 kHz and 100 MHz for a DC bias voltages V_b within the range of 4.0 to 7.36 V. The results are given in Table 1. In Fig. we show the measured impedance magnitude and phase responses for V_b = 7.36 V. We also show fitted the curve (red) using the small signal model shown in Fig. Note that, the estimated PLED parameters are given below in Table I.

Table I Extracted PLED parameters

V_b (V)	R_s (Ω)	R_p(Ω)	C_p (nF)
4.00	92.60	6307.40	1.13
4.98	92.60	2994.40	1.13
5.96	92.60	1740.90	1.13
6.91	92.60	933.50	1.13
7.36	92.60	688.40	1.13

It has been observed that both R_s and C_p remain constant across all bias voltage range adopted in the measurement, while only R_p changes. This can be explained by R_s and C_p both being constant and independent of V_b, see (2); however, the bulk resistance R_p displays a dependence on V_b as reflected in (1). This dynamic behaviour on R_p can also be observed through the inverse of the tangent on the exponential I-V characteristics shown in Fig. 2(b) and (d).

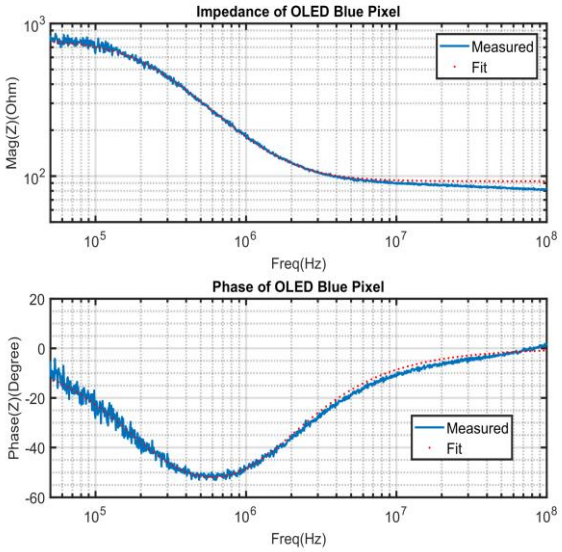

Fig. 4 Impedance magnitude and phase response of the blue pixel PLED biased at 7.36 V

The optical power-current and current-voltage (L-I-V) characteristics, shown in Fig. 2, are important to identify the linear operating region for correct biasing of the devices, which is very important in multi-carrier and multi-level modulation schemes (i.e., OFDM, etc.).

IV. Bandwidth Stability over Time

Whereas PLEDs operational lifetimes tests have appeared as early as 1994 [14] however, one aspect of PLED stability that has not been documented until now is the bandwidth response as a function of the time of operation. This has been investigated in this work by measuring the rise time for each PLED. The system block diagram for the experimental setup is shown in Fig. 5. A pulsed waveform (100 kHz @ 20 % duty cycle and a 2 mA drive current) is applied to the PLED (i.e., intensity modulation) and is buffered to each pixel via independent open-collector NAND gates (74LS03N). The optical output signals are captured using an optical receiver, which is composed of a PIN photodetector (PD- OSD15-5T) with a bandwidth of 29 MHz, and a transimpedance amplifier (TIA) with a bandwidth of 240 MHz and a gain of 90 Ω. The output of the TIA is captured using a digital storage oscilloscope (DSO9254A), whereby the rise time t_r is measured over an average of >10^3 measurements at regular 30-minute intervals. The tests were repeated after several days, and the results were compared.

The B_{mod} of the DUT in terms of t_r, which corresponds to a 1- or 2-pole filter roll-off in the frequency domain, is given by:

$$B_{mod} = 0.35 t_r^{-1} \quad (4)$$

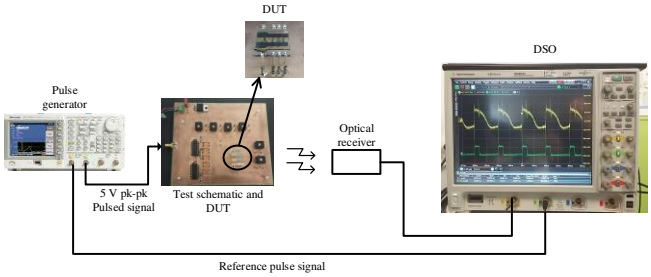

Fig. 5 Simplified rise time experimental measurement setup

The results of the experiments are illustrated in Fig. 6, which shows that the bandwidth of the devices deteriorate over the first few hours of its operation, before reaching an asymptotic steady state value. For the blue PLED, see Fig. 6(a), an initial B_{mod} of approximately 800 kHz is observed, which tails off to a value cantered between ~2 – 300 kHz, which is then essentially stable. Likewise, the green PLED exhibits a similar behaviour Fig. 6(b). An initial B_{mod} of > 1 MHz was recorded, before reaching a stable state at ~800 – 1000 kHz. The devices were then left unused for several days and the experiment was repeated again. Interestingly, the blue PLED (Fig. 6(c)) exhibited a degree of recovery, returning to its initial approximate B_{mod}. Subsequently, similar stable-state B_{mod} occurred after several hours of operation. In contrast, the B_{mod} of green device (Fig. 6(d)) did not recover to its initial value, and remind in the same range of ~800 – 1000 kHz observed after 50 minutes of operation in test 1 (Fig. 6(b)). These measurements clearly demonstrate that, the R_b selected in an organic-based VLC system must be carefully designed according to the stable-state B_{mod}, which has been the methodology adopted in our previous work in [4], and not the initially measured value.

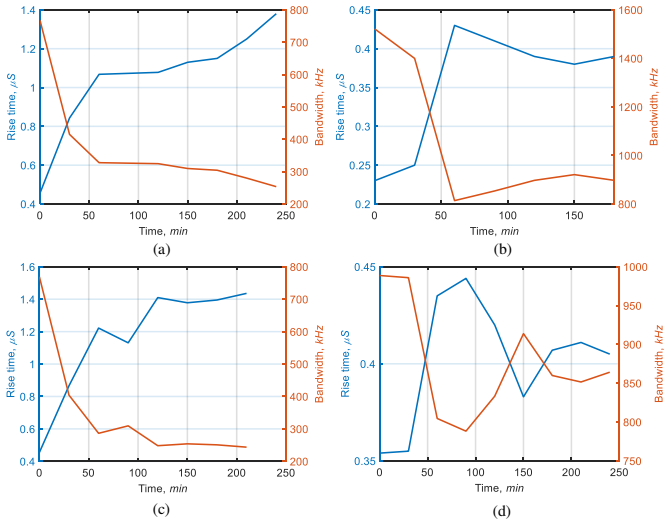

Fig. 6 Experimental t_r results for: (a) blue test 1, (b) green test 1, (c) blue test 2 and (d) green test 2

V. PLED Data Transfer in VLC

This section covers the use of the blue PLED in VLC. The system describes a link using the pulse-based OOK-NRZ modulation with and without the use of a first-order passive RC-equaliser [15]. The driving circuit based on the PNP-BJT current mirror, where all 6 pixels are driven simultaneously and is illustrated in Fig. 7. The input signal $v_{in}(t)$ has been AC coupled into the driver via C_{in}. The potential divider of R_1 and R_2 set both the output bias current (2 mA) and input impedance (50 Ω) of the circuit simultaneously. The input impedance has been set to ensure perfect match with the signal generator.

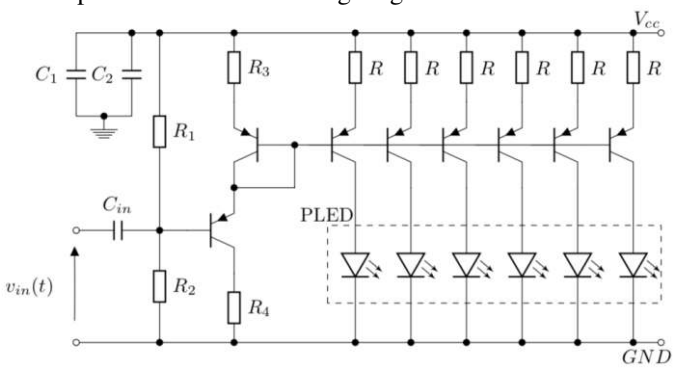

Fig. 7 The driver circuit for the six-pixel PLEDs

A. RC Equalisation

The equalisers have been designed in the following manner. The capacitor values were co-selected with the resistor, based on making the capacitor reactance X_C equal to the resistance R at the DUT bandwidth. The values are listed inset in Fig. 8, where the frequency responses are illustrated, and each plot has been normalised to 0 dB. Each equaliser tested was placed in series between the signal generator and the input to the Tx circuit (the equaliser circuit shown in the insert of Fig. 8). For the measurements, we adopted the 2nd equaliser since it displays the best frequency response in terms of lower baseline wander effect and a wide bandwidth of ~750 kHz, an improvement of 3 times compared to the stable-state bandwidth of ~250 kHz measured for the blue PLEDs.

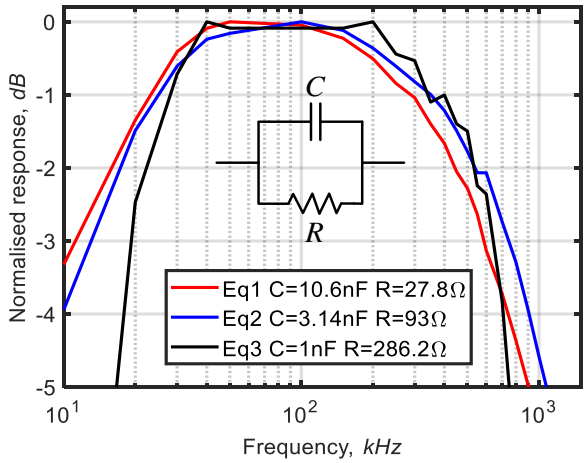

Fig. 8 The raw and equalised frequency response (equaliser circuit inset)

B. System response

A pseudo random bit stream (PRBS) of length 2^{10}-1 was transmitted at speeds of 1 and 2 Mb/s using a Tektronix arbitrary function generator (AFG) to drive the PLEDS. The intensity modulated light signals were converted back into an electrical signal using the same optical receiver as in Section IV, the output of which was captured using a digital scope for post-processing. The captured eye-diagrams for the PLED VLC link with and without the equaliser are shown in Fig. 9. The eye diagrams are used to estimate the quality of the received signal in terms of the Q-factor and the bit error rate (BER) performance. The Q-factor is defined by [16]:

$$Q = \frac{\mu_1 - \mu_0}{\sigma_1 + \sigma_0}, \tag{5}$$

where μ_1 and μ_0 are the mean value for the received signal levels representing 1- and 0-levels, respectively, and σ_1 and σ_1 are the standard deviation for the received 1 and 0-levels respectively. Likewise, the statistical BER is given by:

$$BER = 0.5erfc\left(\frac{Q}{\sqrt{2}}\right), \tag{6}$$

where *erfc* is the complementary error function [16]. The key results for the Q-factor and the BER for equalized and unequalised PLED VLC link are given in Table II.

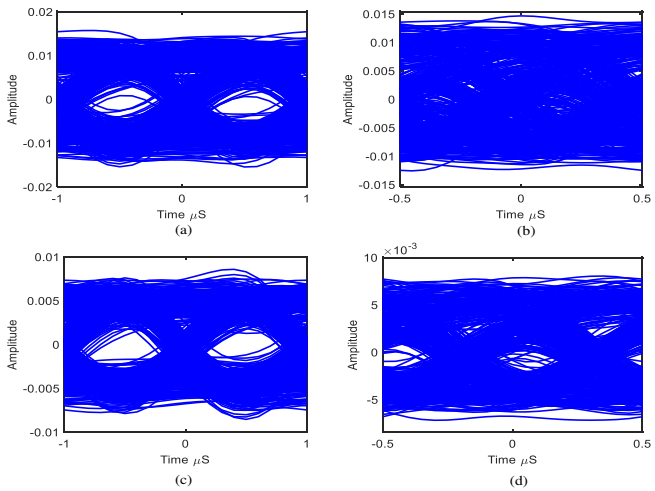

Fig. 9 (a) 1 Mbps no equaliser (1 MHz LPF), (b) 2 Mbps no equaliser (2 MHz LPF), (c) 1 Mbps equaliser 2 (1 MHz LPF) and (d) 2 Mbps equaliser 2 (2 MHz LPF)

Table II Data transmission results

Signal	**Q-factor**		**Statistical BER**	
	1 Mbps	2 Mbps	1 Mbps	2 Mbps
Non equalised	3.14	1.72	8.38e-04	4.24e-2
Equalised	3.40	2.00	3.35e-4	2.26e-2

VI. Conclusion

This paper described the fabrication and characterisation of a new generation of organic PLEDs for used as an optical transmitter in VLC systems. The PLED devices were fully characterised in terms of their L-I-V and the spectral output. The small signal equivalent circuit analysis was performed, which enabled a deeper understanding of the electrical characteristics, and modelling the devices as lumped elements. We investigated the rise time and bandwidth relationship of the fabricated devices and showed that the deterioration in bandwidth over the first hour of operation until a steady state was reached. We also showed a recovery in the bandwidth if the devices were left unoperational for a couple of days, followed by the reduction to the steady state level. When used within the context of a VLC system, we showed that the devices steady state bandwidth tripled by using a simple *RC* equaliser, where we achieved a transmission data rate of >1 Mb/s.

Acknowledgment

This work was supported by the UK EPSRC grant EP/P006280/1: Multifunctional Polymer Light-Emitting Diodes with Visible Light Communications (MARVEL) and the EU H2020 Marie Slodowska-Curie grant agreement no 764461 (VISION). The author Franco Cacialli is a Royal Society Wolfson Foundation Research Merit Award holder.

References

[1] X. Gu, Y. Zhou, K. Gu, T. Kurosawa, Y. Guo, Y. Li, *et al.*, "Roll-to-Roll Printed Large-Area All-Polymer Solar Cells with 5% Efficiency Based on a Low Crystallinity Conjugated Polymer Blend," *Advanced Energy Materials,* vol. 7, p. 1602742, 2017.

[2] T.-Q. Nguyen, R. C. Kwong, M. E. Thompson, and B. J. Schwartz, "Improving the performance of conjugated polymer-based devices by control of interchain interactions and polymer film morphology," *Applied Physics Letters,* vol. 76, pp. 2454-2456, 2000.

[3] I. A. Barlow, T. Kreouzis, and D. G. Lidzey, "High-speed electroluminescence modulation of a conjugated-polymer light emitting diode," *Applied Physics Letters,* vol. 94, p. 162, 2009.

[4] P. A. Haigh, F. Bausi, H. Le Minh, I. Papakonstantinou, W. O. Popoola, A. Burton, *et al.*, "Wavelength-Multiplexed Polymer LEDs: Towards 55 Mb/s Organic Visible Light Communications," *IEEE Journal on Selected Areas in Communications,* vol. 33, pp. 1819-1828, Sep 2015.

[5] H. J. Chen, Z. Y. Xu, Q. Gao, and S. B. Li, "A 51.6 Mb/s Experimental VLC System Using a Monochromic Organic LED," *IEEE Photonics Journal,* vol. 10, pp. 1-12, Apr 2018.

[6] T. M. Brown and F. Cacialli, "Contact optimization in polymer light-emitting diodes," *Journal of Polymer Science Part B,* vol. 41, pp. 2649-2664, 2003.

[7] T. M. Brown, G. M. Lazzerini, L. J. Parrott, V. Bodrozic, L. Bürgi, and F. Cacialli, "Time dependence and freezing-in of the electrode oxygen plasma-induced work function enhancement in polymer semiconductor heterostructures," *Organic Electronics,* vol. 12, pp. 623-633, 2011/04/01/ 2011.

[8] E. J. W. List, R. Guentner, P. Scanducci de Freitas, and U. Scherf, "The Effect of Keto Defect Sites on the Emission Properties of Polyfluorene-Type Materials," *Advanced Materials,* vol. 14, pp. 374-378, 2002.

[9] K. Becker, J. M. Lupton, J. Feldmann, B. S. Nehls, F. Galbrecht, D. Q. Gao, *et al.*, "On-Chain Fluorenone Defect Emission from Single Polyfluorene Molecules in the Absence of Intermolecular Interactions," *Advanced Functional Materials,* vol. 16, pp. 364-370, 2006.

[10] A. Zampetti, A. Minotto, B. M. Squeo, V. G. Gregoriou, S. Allard, U. Scherf, *et al.*, "Highly Efficient Solid-State Near-infrared Organic Light-Emitting Diodes incorporating A-D-A Dyes based on α,β-unsubstituted "BODIPY" Moieties," *Scientific Reports,* vol. 7, p. 1611, 2017/05/09 2017.

[11] M. Ellen, "Conjugated polymer blends: linking film morphology to performance of light emitting diodes and photodiodes," *Journal of Physics: Condensed Matter,* vol. 14, p. 12235, 2002.

[12] J. C. de Mello, H. F. Wittmann, and R. H. Friend, "An improved experimental determination of external photoluminescence quantum efficiency," *Advanced Materials,* vol. 9, pp. 230-232, 1997.

[13] P. Horowitz and W. Hill, *The art of electronics*: Cambridge Univ. Press, 1989.

[14] F. Cacialli, R. H. Friend, S. C. Moratti, and A. B. Holmes, "Characterization of Properties of Polymeric Light-Emitting-Diodes over Extended periods," *Synthetic Metals,* vol. 67, pp. 157-160, 1994.

[15] H. Le Minh, Z. Ghassemlooy, A. Burton, and P. A. Haigh, "Equalization for organic light emitting diodes in visible light communications," in *GLOBECOM Workshops (GC Wkshps), 2011 IEEE*, 2011, pp. 828-832.

[16] Z. Ghassemlooy, L. N. Alves, M. A. Khalighi, and S. Zvanovec, *Visible Light Communications: Theory and Applications*: Taylor & Francis Incorporated, 2017.